Catalysis Science & Technology

ROYAL SOCIETY OF CHEMISTRY

PAPER

View Article Online
View Journal

Cite this: DOI: 10.1039/d5cy01600b

Pt–Re dehydrogenation catalysts synthesized *via* solvent deficient precipitation

Ana de Oliveira,[ab] Felix Lederle,[cd] Philipp Memmel,[cd] Eike G. Hübner,[cd] Peter Wasserscheid,[abe] Moritz Wolf[f] and Franziska Auer *[a]

Received 28th December 2025,
Accepted 16th March 2026

DOI: 10.1039/d5cy01600b

rsc.li/catalysis

This study demonstrates the feasibility of producing Pt–Re/Al_2O_3 catalysts *via* the scalable solvent deficient precipitation method achieving enhanced performance in the dehydrogenation of liquid organic hydrogen carriers. Effects similar to wet impregnated Pt–Re catalysts were observed, indicating the transferability of the Re promotion concept across catalyst synthesis approaches. In continuous gas-phase dehydrogenation of methyl cyclohexane, Re addition improved the Pt-based activity, selectivity, and stability, while reducing coking and effective activation energy. For perhydro benzyltoluene dehydrogenation, Re increased catalyst activity across various loadings with a molar ratio of Re/Pt = 0.5 yielding the highest hydrogen production rate. Higher Re loadings led to a rapid performance decline due to side reactions and catalyst deactivation, likely caused by deep dehydrogenation pathways and strong binding of the dehydrogenated product benzyltoluene to the active sites. Kinetic studies revealed that Re reduces the effective activation energy, although diffusional limitations were observed due to the small pore sizes of the produced catalyst materials. Successful 10-fold scale-up of the solvent-deficient precipitation was achieved without water, binders, or additives with performances comparable to small-scale syntheses. This highlights the potential of this simple, cost-effective, and scalable approach for the high-throughput production of bimetallic Pt-based catalysts.

1. Introduction

In the context of green hydrogen supply for the energy sector, liquid organic hydrogen carriers (LOHCs) offer a promising solution for hydrogen storage and long-range transportation by reversibly binding H_2 to storage molecules such as aromatic hydrocarbons through hydrogenation/dehydrogenation reactions.[1,2] This technology is scalable and compatible with existing fuel transportation infrastructure, as LOHCs possess similar physical properties to fossil fuels.[3–6] Examples of LOHC pairs include methyl cyclohexane (MCH, H_2-rich) and toluene (TOL, H_2-lean), which are widely used solvents in the chemical industry, as well as perhydro benzyltoluene (H12-BT, H_2-rich) and benzyltoluene (H0-BT, H_2-lean), the latter being broadly utilised as heat transfer fluid.[2,5] The hydrogen-loaded molecules enable safe and loss-free storage as liquids under atmospheric conditions of pressure and temperature, posing minimal safety risks, while hydrogen can be released on-site and on demand with high purity.[5]

The cyclic loading and unloading of the LOHC molecules occurs through catalytic hydrogenation and dehydrogenation processes, which can be repeated multiple times.[5–8] These reactions are highly dependent on the efficiency of the catalysts, with platinum (Pt) being one of the most suitable active metals for hydrogen release from homocyclic LOHC molecules owing to its high selectivity for C–H bond cleavage.[9] Furthermore, minimizing side product formation is crucial, as it facilitates the reloading of the resulting product mixture and ensures the circularity of the carrier molecule.[5,9]

Under the demanding conditions of power-dense dehydrogenation reactors, Pt-based catalysts are prone to deactivation through sintering and coking, as well as catalysing undesired side reactions. To mitigate this, adjusting the catalyst properties is essential, as improved Pt dispersion and electronic configuration can ensure a stable and robust active material.[10] This can be achieved through

[a] Forschungszentrum Jülich GmbH, Helmholtz Institute Erlangen-Nürnberg for Renewable Energy (IET-2), Erlangen, Germany. E-mail: f.auer@fz-juelich.de
[b] Department of Chemical Reaction, Friedrich-Alexander-University Erlangen-Nürnberg, Erlangen, Germany
[c] Clausthal University of Technology, Institute of Organic Chemistry, Clausthal-Zellerfeld, Germany
[d] Fraunhofer Institute for Telecommunications, Heinrich-Hertz-Institut, HHI, Fiber Optical Sensor Systems, Goslar, Germany
[e] Forschungszentrum Jülich GmbH, Institute for a Sustainable Hydrogen Economy (IHE), Jülich, Germany
[f] Karlsruhe Institute of Technology (KIT), Engler-Bunte-Institut & Institute of Catalysis Research and Technology, Karlsruhe, Germany

the addition of promoters, which introduce geometric and electronic modifications that can enhance catalyst activity, selectivity, and stability.[11] Such a beneficial ensemble effect has been reported for Pt–Re catalysts in MCH dehydrogenation, where the presence of Re reduces catalyst deactivation and increases the stability by altering the nature of the coke formed, making it less carboxylic.[12–14] In H12-BT dehydrogenation, Pt–Re/Al_2O_3 catalysts outperformed the monometallic counterpart, achieving higher Pt-based H_2 production rates, which was attributed to a modified reaction mechanism favouring fully dehydrogenated species (H0-BT) over partially hydrogenated (H6-BT) molecules.[15]

Nevertheless, successful modifications of Pt-based catalysts depend on the synthesis method. The latter is known to significantly influence key material properties, such as structure and surface chemistry.[5] Solid-state syntheses, which involve nucleation and growth processes, have been employed to prepare catalyst supports and simplify aqueous-based synthesis methods, such as wet impregnation (WI). A notable example is the solvent-deficient precipitation (SDP) method developed by Woodfield *et al.*,[16] which is a simple and versatile approach for preparing mesoporous mixed-metal oxide nanoparticles. This method uses only a metal salt (such as chloride or nitrate) and a base, such as ammonium (bi)carbonate or hydroxide (*e.g.*, NH_4HCO_3).[17] Initially, these solid precursors are mixed and ground for a few minutes, followed by calcination to form the metal oxide. By simply adding an active metal precursor to the mixture, metal oxide supported catalysts can be prepared. The solvent-free conditions not only reduce catalyst preparation times and significantly lower production costs, they also result in small, uniformly distributed nanoparticles, which are beneficial for improving the catalytic performance.[18]

Due to the versatility of this synthesis method, it has been successfully applied to prepare catalysts for the dehydrogenation of perhydro 2-(*N*-methylbenzyl)pyridine, perhydro dibenzyltoluene (H18-BT) and H12-BT, where the catalysts even outperformed their counterparts synthesised by WI.[9,19] Additionally, the incorporation of secondary elements, such as sulphur and manganese, into Pt-based catalysts through the SDP method has been shown to produce effects similar to those achieved with WI catalysts.[20,21]

This study focuses on synthesising Pt-based catalysts modified with Re *via* the SDP method to enhance H_2 release from MCH. The performance of Pt–Re/Al_2O_3 catalysts is evaluated using continuous MCH gas phase dehydrogenation in the temperature range between 240 and 320 °C. For comparison, the dehydrogenation of liquid H12-BT in semi-batch mode at 250 °C with the same catalysts is discussed. Catalytic properties are assessed through microscopic characterisation and CO-pulse chemisorption. Additionally, successful scaling up of the synthesis without the use of surfactants, additives, or binders is demonstrated.

2. Methodology

Materials

The compounds utilised to prepare the catalysts, namely aluminium nitrate nonahydrate (>98% purity), ammonium perrhenate(VII) ($(NH_4)ReO_4$, 99.999% purity), tetraamine platinum(II) nitrate ($Pt(NH_3)_4(NO_3)_2$, 99.99% purity), were supplied by Thermo Scientific and used as received. For dehydrogenation experiments, methyl cyclohexane (MCH, 99% purity) was purchased from Thermo Scientific and perhydro benzyltoluene (H12-BT, 98% purity) was supplied by Hydrogenious LOHC Technologies GmbH (https://www.hydrogenious.net).

Preparation of catalysts

Pt-based catalysts on a γ-Al_2O_3 mesoporous support were prepared following the SDP method. Single batches of 3 g were synthesised by mixing 0.02 g of $Pt(NH_3)_4(NO_3)_2$, 21 g of $Al(NO_3)_3{\cdot}9H_2O$ and 14 g of NH_4HCO_3 in a mortar, followed by grinding by hand with a pestle. For Pt–Re/Al_2O_3 catalysts, $(NH_4)ReO_4$ was simultaneously added in desired proportions, maintaining a fixed molar ratio of 1 between total nitrate and ammonium hydrogen carbonate to ensure a stoichiometric reaction. During mixing, the reactants liquefied and bubbled vigorously due to hydration water and CO_2 release. The end of this phase was marked by the absence of bubbles resulting in a slurry-like final mixture, indicating the precipitation of metal oxide precursors as depicted in Fig. 1. The resulting wet solid was calcined in a muffle oven from Nabertherm at 600 °C (temperature ramp: 2 K min^{-1}) for 1 h with a synthetic air flow of 10 L min^{-1}. The final solid was again ground for 30 seconds in a mortar to yield a fine powder. Finally, the catalyst was reduced in a quartz tube inside a tubular furnace from Carbolite at 400 °C (temperature ramp: 12.67 K min^{-1}) under 10 vol% H_2/N_2 at a total flow rate of 500 mL min^{-1} for 1 h.

Scaled batch sizes

For the production of larger batches of the catalyst in a semi-automatic process, the SDP synthesis was carried out in a 5 L three-necked round-bottom flask with a permanently attached KPG stirrer (Fig. 2). Stoichiometric amounts of NH_4HCO_3 were slowly added to the entire amount of $Al(NO_3)_3{\cdot}9H_2O$ as a fine powder while stirring continuously. $Pt(NH_3)_4(NO_3)_2$ and $(NH_4)ReO_4$ were added, if appropriate, and the mixture was stirred for several hours. A transformation of the mixture in different stages could be observed *via* a thick slurry, a thin liquid, a sticky material, and finally a moist paste. During the reaction process, a significant cooling of the mixture below 0 °C was observed. The reaction is complete once a slurry-like consistency is achieved. With around four hours, the reaction time is significantly longer than for the small-scale synthesis described above. The moist slurry was freeze-dried in a beta 1–8 freeze dryer (Martin Christ GmbH). Drying was carried

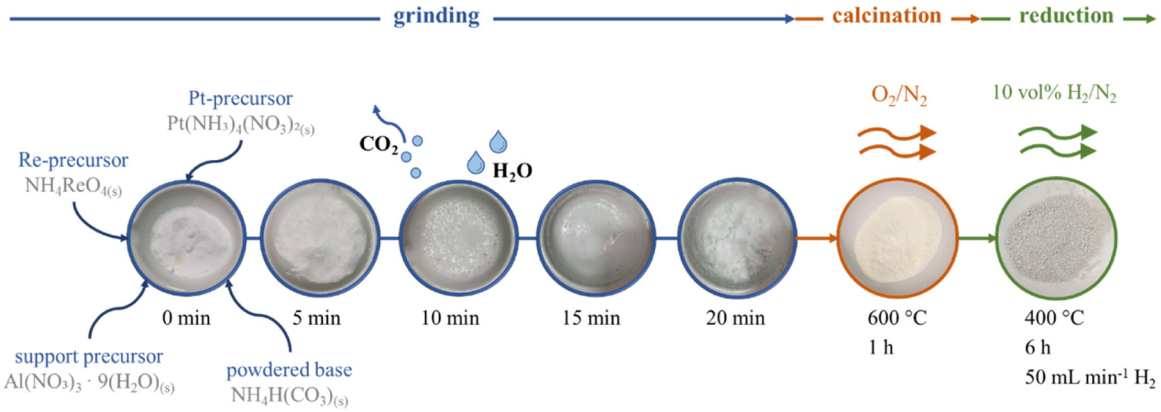

Fig. 1 Summary of synthesis of a Pt–Re/Al_2O_3 *via* the solvent deficient precipitation (SDP) method, showing the grinding, calcination and reduction steps.

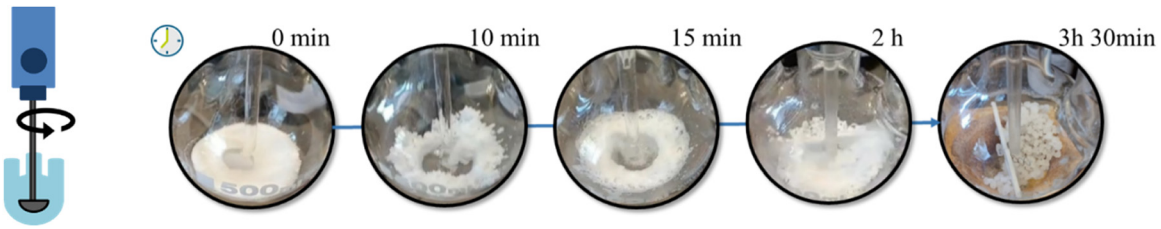

Fig. 2 Mixing stages during the solvent deficient precipitation (SDP) synthesis of 3 g of Pt/Al_2O_3 using a core drawn precision glassware (KPG) mixer.

out in two steps at −30 °C and 0.3 mbar for 84 hours and then at −55 °C and 0.08 mbar for 12 hours. Calcination was carried out in evaporation dishes in a muffle furnace (Nabertherm L 9/13 B150) at a constant air flow of 10 L min^{-1} at 600 °C (heating rate 1.2 K min^{-1}). Adequate ventilation was ensured to remove any nitrous gases produced. The reduction was carried out in small batches according to the procedure described above, followed by recombination and homogenisation. Example weigh-ins for the preparation of 40 g Pt/Al_2O_3 are 293.5 g (0.78 mol) $Al(NO_3)_3{\cdot}9H_2O$, 185.7 g (2.35 mol) NH_4HCO_3, 0.238 g (0.615 mmol) $Pt(NH_3)_4(NO_3)_2$.

Characterisation of catalysts

The metal loadings of the prepared catalysts were determined by means of inductively coupled plasma with optical emission spectroscopy (ICP-OES), using a Ciros CCD from Spectro Analytical Instruments GmbH. The samples were prepared by mixing approximately 200 mg with 10 mL of concentrated *aqua regia* (volumetric ratio $HCl:HNO_3 = 3:2$) and subjected to microwave digestion at 200 °C for 30 min. Prior to measurements, the instrument was calibrated using standard solutions of the target elements, and the characteristic lines evaluated were 167.020 nm for Al, 214.423 nm for Pt, 221.426 nm for Re.

The textural properties of the supports and catalysts were evaluated by means of low temperature N_2 physisorption using a TriStar II Plus from Micromeritics. The samples were degassed overnight at 250 °C in vacuum. The specific surface area was calculated *via* the Brunauer–Emmett–Teller (BET) method for a relative pressure range p/p_0 of 0.05 to 0.35. The pore size distribution was obtained according to the Barrett–Joyner–Halenda (BJH) model for cylindrical pores from the desorption curve of the physisorption isotherm. Considering an uniform cylindrical shape for all pores, the average pore diameter of the catalytic systems, $d_{average}$, was estimated by eqn (1), where S_{BET} represents the BET specific surface area and $V_{BJH,cumulative}$, the cumulative pore volume calculated *via* the BHJ method.

$$d_{average} = 4\frac{V_{BJH,cumulative}}{S_{BET}} \quad (1)$$

The particle size distribution (PSD) of Pt particles in the synthesised catalysts was analysed using conventional and high-resolution transmission electron microscopy (TEM), high-angle annular dark field scanning TEM (HAADF-STEM) and energy-dispersive X-ray spectroscopy (EDXS) for elemental mapping of Pt and Re. Samples were prepared by dispersing the catalyst in ethanol *via* ultrasonication and depositing a few droplets onto a Cu-carbon grid. Imaging was performed with a Thermo Fisher Scientific Talos F200i microscope equipped with a Schottky emitter and two Bruker XFlash 6T-100 EDS detectors, operated at 200 kV. Data evaluation was performed using the Velox software and Pt particle diameters were determined from HAADF images

using the open-source software Fiji ImageJ.[22] The average particle size was calculated using the volume–area diameter equation (*i.e.* Sauter mean diameter),[23] represented in eqn (2), where d_i represents the particle diameter and n_i is the corresponding particle count (at least 75 particles).

$$d_{VA}\,[\mathrm{nm}] = \frac{\sum n_i {d_i}^3}{\sum n_i {d_i}^2} \tag{2}$$

The metallic active centres in the synthesised catalysts were evaluated *via* CO pulse chemisorption. First, all materials were reduced *in situ* under 5 vol% of H_2 in Ar at 400 °C for 60 min. Following this, successive pulses of 0.5117 mL_N of CO/He were injected at 35 °C into the sample chamber until the catalyst surface was saturated (*i.e.* no change in TCD signal). Subsequently, a temperature-programmed desorption (TPD) was conducted by heating the sample to 300 °C (temperature rate: 15 °C min^{-1}) under He, recording the desorbed amount of CO. It was considered that 1 mol of CO adsorbs onto 1 mol of available Pt.

The coke content of the spent SDP catalysts in the dehydrogenation of MCH was quantified *via* temperature-programmed oxidation (TPO). The weight change was monitored by means of thermogravimetric analysis (TGA) using a TGA 8000 from Perkin Elmer. A sample mass within the range of 5 to 20 mg was placed in a ceramic crucible, heated to 120 °C (heating rate: 10 K min^{-1}), and held for 30 min under an inert atmosphere of N_2 to remove physisorbed molecules. Subsequently, the sample was heated to 1000 °C (heating rate: 50 K min^{-1}) and held for 10 min to guarantee the complete oxidation of all carbonaceous deposits in 21% O_2/N_2. The overall flow rate was 50 mL min^{-1} throughout the TPO. The mass loss in the final temperature ramp and at 1000 °C was compared to the sample mass after 2 h at 120 °C to assess to coke content.

Catalytic testing in the gas phase

Continuous gas-phase dehydrogenation of MCH was performed in a tubular inconel reactor (diameter: 9.26 mm, length: 60 cm) loaded with 1.0 g of catalyst, which was positioned between two plugs of glass wool in the middle of the reactor. The testing set-up is described in detail elsewhere.[24] The reactor was heated to the desired reaction temperature and a programmed temperature variation between 240 and 320 °C was conducted for catalyst testing at 1 bara. The inlet gas mixture, consisting of 57 mL min^{-1} He and 0.05 g mL^{-1} liquid MCH, was regulated by Bronkhorst MFCs. MCH was vapourised at 200 °C using an evaporator, and all subsequent connecting lines were maintained at this temperature to prevent condensation. The mean residence time was approximately 0.6 s and the weight hourly space velocity (WHSV) was 8.31 $L_{gas}\ g_{cat}^{-1}\ h^{-1}$.

The outlet gas composition was analysed in a mini-GC 7820 A from Agilent Technologies equipped with an FID. Separation was achieved in a Restek Rtx-100-DHA column (diameter: 250 μm, length: 105 m). The molar fraction of each species was calculated based on the peak areas. The conversion of MCH X_{MCH} was calculated from the total peak area A_{total} and the peak area corresponding to unreacted MCH A_{MCH}, as shown in eqn (3).

$$X_{MCH} = \frac{A_{total} - A_{MCH}}{A_{total}} \tag{3}$$

The selectivity of toluene S_{TOL} was obtained based on the toluene peak area A_{TOL} in comparison to the total peak area excluding the one for MCH, as shown in eqn (4).

$$S_{TOL} = \frac{A_{TOL}}{A_{total} - A_{MCH}} \tag{4}$$

Toluene productivity $Prod_{TOL}$ was calculated from the converted amount of MCH $\dot{n}_{MCH,0}$, toluene selectivity and its molar mass M_{TOL}, as well as the Pt mass in the catalyst bed m_{Pt}, as described in eqn (5). Cumulative productivity Cum $Prod_{TOL,i}$ was determined by integrating the productivity over a specific time interval t as indicated in eqn (6).

$$\mathrm{Prod}_{TOL} = \frac{x_{MCH}\cdot\dot{n}_{MCH,0}\cdot S_{TOL}\cdot M_{TOL}}{m_{Pt}} \tag{5}$$

$$\mathrm{Cum\ Prod}_{TOL,i} = \int_0^t P_{TOL,i}\,\mathrm{d}t \tag{6}$$

Toluene selectivity exceeded 98% for all experiments. Assuming an ideal reaction where 3 mols of H_2 are released per mol of MCH, as shown in Fig. 3, the amount of released hydrogen $\dot{n}_{H_2}$ was calculated based on the produced TOL, as described in eqn (7). Thus, the productivity of H_2 was calculated according to eqn (8).

$$\dot{n}_{H_2} = 3\dot{n}_{TOL} \tag{7}$$

$$P_{H_2,i} = \frac{3\cdot\left(x_{MCH}\cdot\dot{n}_{MCH,0}\cdot S_{TOL}\right)\cdot M_{H_2}}{m_{Pt}} \tag{8}$$

The dehydrogenation equilibrium of MCH was simulated *via* Gibbs free energy minimisation using the software Aspen Plus[25] to compare with experimental results. The Predictive Redlich Kwong–Soave (PSRK) property method was chosen for gas processing. A sensitivity analysis was performed over a range of temperatures between 240 and 320 °C at 1 bara mirroring the lab experiments.

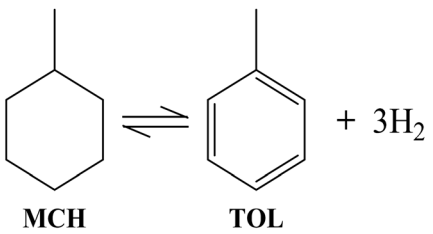

Fig. 3 Reaction equation for the dehydrogenation of methylcyclohexane (MCH) to the desired product toluene (TOL).

Catalytic testing in the liquid phase

Semi-batch liquid-phase dehydrogenation experiments were conducted in a four-neck round-bottom flask with 0.1 mol of H12-BT (19.5 g) as feedstock. The system was supplied with an Ar flow of 300 $mL_N\ min^{-1}$, controlled by a MFC from Bronkhorst, for inertisation, and temperature was set to 250 °C with a heating mantle from Heraeus–Wittmann and a Fitron TP controller from Fiege. The catalyst was added through a metallic dispensing tool after reaching the target temperature. A condenser operating at −5 °C was used to condense and reflux Hx-BT species, with the outlet stream passing through a sulphuric acid bubbler and an active carbon filter to prevent interference or damage to the H_2 analyser. Hydrogen concentration was continuously monitored using a calibrated FTC 300 thermal conductivity detector (TCD) from Messkonzept. Standard experiments used 0.3 wt% Pt catalysts with a molar ratio between Pt and LOHC of 0.0001 $mol_{Pt}\ mol_{LOHC}^{-1}$.

The volumetric flow rate of H_2 $\dot{V}_{H_2}$ was obtained from the H_2 concentration φ_{H_2} given by the TCD in ppm, according to eqn (9), while the cumulative volume of H_2 $V_{H_2,t}$ was calculated *via* eqn (10).

$$\dot{V}_{H_2}\left[\text{mL min}^{-1}\right] = \frac{\varphi_{H_2}\cdot\dot{V}_{Ar}\cdot 10^{-6}}{1-\varphi_{H_2}\cdot 10^{-6}} \quad (9)$$

$$V_{H_2,t}\,[\text{mL}] = \frac{\dot{V}_{H_2,t}\left[\text{mL min}^{-1}\right]}{60\left[\text{s min}^{-1}\right]}\Delta t[\text{s}] + \sum_{0}^{t-1} V_{H_2,t}\,[\text{mL}] \quad (10)$$

The degree of dehydrogenation DoDh was obtained from the ratio of released H_2 volume and the maximum theoretically releasable amount of H_2 V_{max}, following eqn (11).

$$\text{DoDh} = \frac{V_{H_2}}{V_{max}} = \frac{\sum_{0}^{t} V_{H_2,t}}{V_{max,t=0} - \sum_{0}^{t} V_{samples,t}}\cdot 100\% \quad (11)$$

Hydrogen productivity $Prod_{H_2}$ was calculated *via* eqn (12), taking into consideration the H_2 volumetric flow $\dot{V}_{H_2,i}$,H_2 density ρ_{H_2}, Pt loading of the used catalyst w_{Pt} and catalyst mass $m_{catalyst}$.

$$Prod_{H_2,i}(\text{TCD})\left[g_{H_2}\ g_{Pt}^{-1}\ \text{min}^{-1}\right] = \frac{\dot{V}_{H_2,i}\cdot\rho_{H_2}}{w_{Pt}\cdot m_{catalyst}} \quad (12)$$

The liquid phase composition during dehydrogenation was analysed, clustering the LOHC species into five groups: H12-BT (fully hydrogenated reactant), H6-BT (intermediate product), H0-BT (fully dehydrogenated product), and methyl fluorene (MF), as shown in Fig. 4. The formation of MF, which is a undesired side product, serves as marker to evaluate the catalyst selectivity. For this, liquid samples were analysed using a TRACE 1310 gas chromatograph (GC) from Thermo Scientific, equipped with a flame ionisation detector (FID). Separation was achieved with a Rxi17Sil column (diameter: 250 μm, length: 30 m). Samples were prepared by diluting 0.1 mL of taken sample with 0.9 mL of isopropanol.

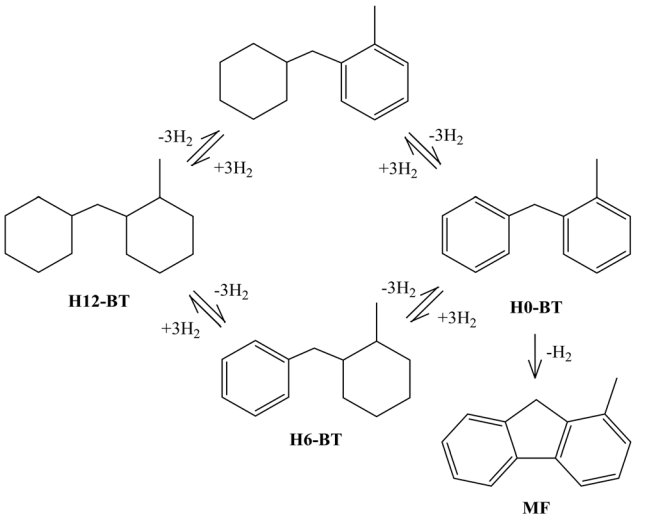

Fig. 4 Reaction paths for the dehydrogenation of perhydro benzyltoluene (H12-BT), including the intermediate H6-BT, desired product H0-BT and undesired side product methylfluorene (MF).

Approximately 2 μL of this mixture were injected for GC analysis.

The molar fraction x_i of each species was determined based on the GC peak areas. The degree of hydrogenation DoH was calculated disregarding dehydrogenated species (*i.e.* H0-BT, MF), as in eqn (13). The DoDh was then derived from the DoH, as shown in eqn (14).

$$\text{DoDh} = 1 - \frac{\frac{12}{12}x_{\text{H12-BT}} + \frac{6}{12}x_{\text{H6-BT}} + \frac{0}{12}x_{\text{H0-BT}} + \frac{0}{12}x_{MF}}{x_{\text{H12-BT}} + x_{\text{H6-BT}} + x_{\text{H0-BT}} + x_{MF}} \quad (13)$$

$$\text{DoDh} = 1 - \text{DoH} \quad (14)$$

The hydrogen productivity based on the GC data was obtained from eqn (15), where ΔDoDh represents the difference of the DoDh between two consecutive liquid samples, $n_{\text{H12-BT},t=0}$ the initial amount of H12-BT, $n_{H_2,\text{per H12-BT}}$ the amount of H_2 mols per H12-BT molecule.

$$Prod_{H_2,i}(\text{GC})\left[g_{H_2}\ g_{Pt}^{-1}\,\text{min}^{-1}\right] = \frac{\Delta\text{DoDh}\cdot n_{\text{H12-BT},t=0}\cdot n_{H_2,\text{per H12-BT}}\cdot M_{H_2}}{m_{Pt}\cdot\Delta t} = \frac{1.2\cdot\Delta\text{DoDh}}{w_{Pt}\cdot m_{catalyst}\cdot\Delta t} \quad (15)$$

3. Results and discussion

Catalyst characterisation

Structural and textural properties. In the following, characterisation data of the Re-free Pt/Al_2O_3 catalyst obtained from the SDP synthesis method is exemplarily shown. XRD analysis of the calcined Pt/Al_2O_3 catalyst (see SI Fig. A1) confirmed the presence of an amorphous γ-Al_2O_3 phase and N_2 physisorption indicated an average BET surface area of 259 $m^2\ g^{-1}$ and an average pore diameter of 6.0 nm (see SI Fig. A2). The corresponding BHJ pore size distribution is shown in Fig. 5. The measured values are in good agreement

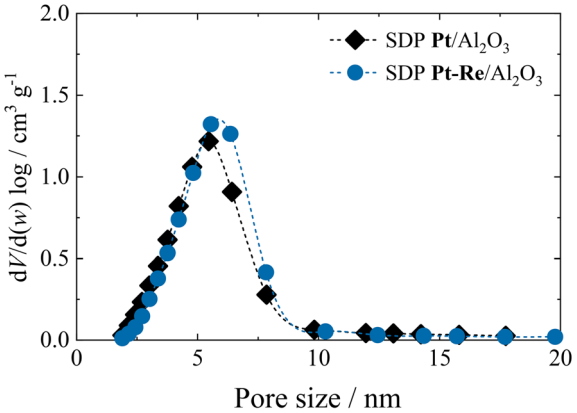

Fig. 5 Pore volume (V_{BHJ}) and pore size distribution (PSD) obtained for Pt/Al_2O_3 (0.3 wt% Pt) and $Pt–Re/Al_2O_3$ (0.3 wt% Pt, 0.27 wt% Re, Re/Pt = 0.88) *via* N_2 physisorption obtained using the adsorption branch.

with the ones reported by Smith *et al.*[17] for γ-Al_2O_3 synthesised *via* the SDP method, namely a specific surface area of 267 $m^2\ g^{-1}$ and an average pore diameter of 4.0 nm.

The structural and textural properties of the Re containing catalyst do not differ significantly from the one without Re. The data of a $Pt–Re/Al_2O_3$ catalyst with Re/Pt = 0.88 is also presented in Fig. 5 (BET surface area of 276 $m^2\ g^{-1}$, average pore diameter of 5.8 nm).

Pt-dispersion. TEM images of a Pt/Al_2O_3 catalyst (0.28 wt% Pt) reveal that the majority of Pt nanoparticles fall within the 1–2 nm diameter range (see Fig. 6), with an average size of 1.8 nm. In contrast, the addition of Re at a molar ratio of Re/Pt = 0.5 (0.31 wt% Pt, 0.14 wt% Re) resulted in smaller particles with an average size of 1.4 nm (see Fig. 7), indicating a higher dispersion. This observation is consistent with previous reports on Pt–Re catalysts synthesised *via* WI, where increasing Re loadings reduced Pt particle size.[15] Nevertheless, further increasing the Re/Pt molar ratio to 3.19 (0.29 wt% Pt, 0.87 wt% Re) yielded an average particle size of 1.8 nm, comparable to that of the monometallic catalyst (see SI Fig. A3). TEM(-EDX) analyses of Pt–Re systems, shown in SI Fig. A4, were limited by low concentrations of Pt and Re, rapid charging of the Al_2O_3 support, and similar atomic numbers of Pt and Re.

Additionally, CO-pulse chemisorption was used to examine the accessibility of Pt surface sites and Pt–Re interactions. As shown in Fig. 8, the catalysts containing Re, especially the one with a Re/Pt ratio of 0.5, exhibited a decrease in chemisorbed CO compared to monometallic Pt. This observation was also reported by Pieck *et al.*,[26] while the mean particle diameter measured by TEM remained nearly unchanged. They found that CO is only adsorbed on Pt surface atoms and concluded an interaction between Pt and Re altering the properties of Pt surface atoms and therefore the CO adsorption capacity.

For the SDP catalysts in this study, TEM pictures also indicate that the addition of low amounts of Re to Pt results in unchanged or slightly reduced average particle sizes, while, contrary to this observation, the CO uptake decreases. According to the literature on WI catalysts, Re might be present as ReO_x as reduction processes conducted below 500 °C are not sufficient to fully reduce Re species. Moreover, previous studies have confirmed that the contribution of ReO_x is negligible in CO-chemisorption at temperatures below 50 °C.[26,27] However, these species could partially cover Pt sites and reduce adsorption relative to pure Pt.[28] Besides this geometric effect, CO adsorption on Pt could also be altered *via* an electronic effect of Re species. In either way, the decreased CO uptake at similar particle sizes in Pt–Re catalysts points towards an interaction between the two compounds.

Dehydrogenation in the gas phase with Pt–Re catalysts

A series of $Pt–Re/Al_2O_3$ catalysts with Re/Pt molar ratios ranging from 0 to 1 was synthesised *via* SDP and tested in

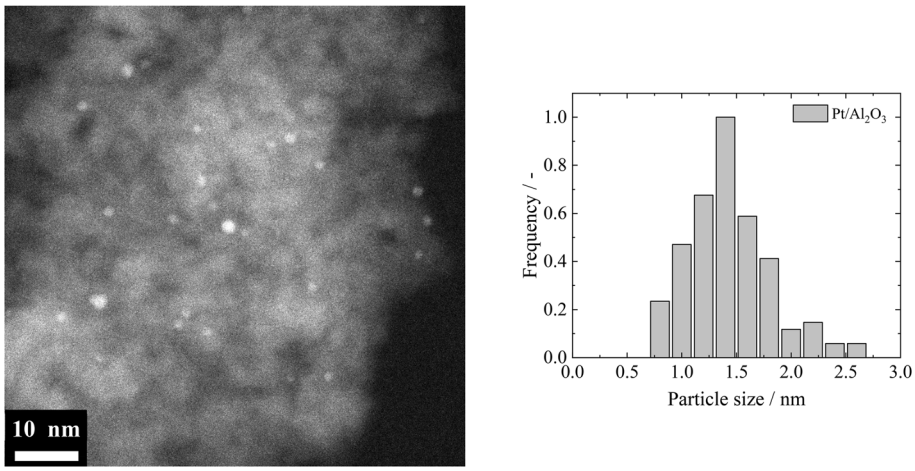

Fig. 6 Representative TEM image of a solvent deficient precipitation (SDP) Pt/Al_2O_3 catalyst (0.28 wt% Pt) showing Pt nanoparticles distributed over γ-Al_2O_3 (left) and corresponding particle size distribution (PSD) based the measurement of 128 particles (right).

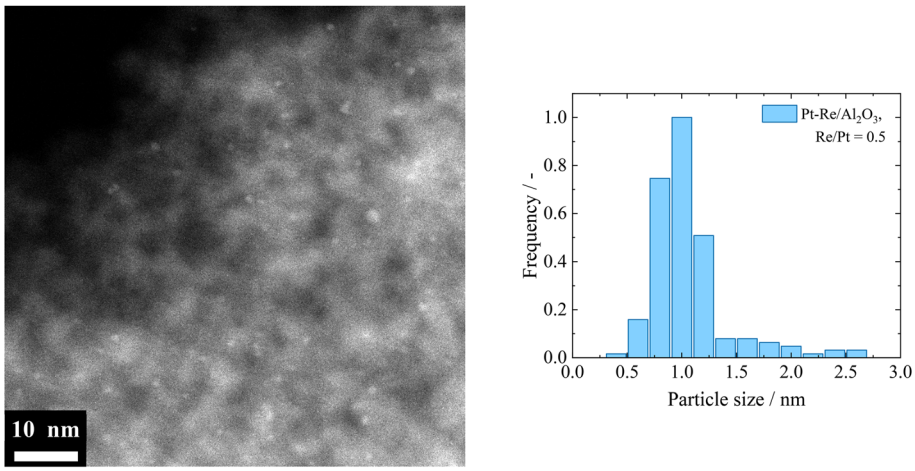

Fig. 7 TEM image of a solvent deficient precipitation (SDP) Pt–Re/Al_2O_3 with Re/Pt = 0.5 (0.31 wt% Pt, 0.14 wt% Re), showing metal nanoparticles distributed over γ-Al_2O_3 (left) and particle size distribution (PSD) based the measurement of 175 particles (right). Due to the low metal loadings, Pt and Re could not be distinguished.

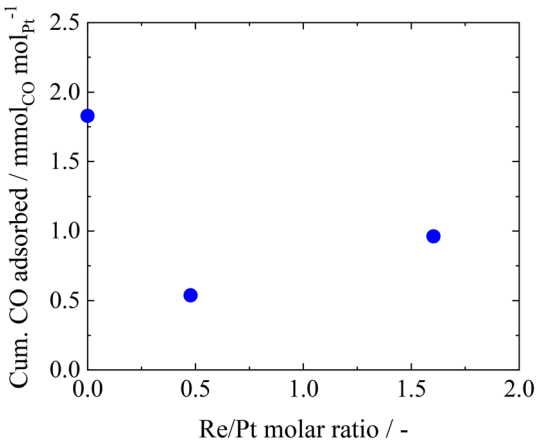

Fig. 8 Cumulative amount of CO adsorbed onto the Pt–Re catalysts with Re/Pt molar ratios of 0 (0.28 wt% Pt), 0.5 (0.31 wt% Pt, 0.14 wt% Re) and 1.6 (0.29 wt% Pt, 0.44 wt% Re).

the continuous gas phase dehydrogenation of MCH. The contents of Pt and Re were measured by means of ICP-OES, which are shown in Table 1. The target values were reached with small deviations for all catalysts.

As shown in Fig. 9, Re addition enhanced both activity and selectivity. After 10 hours of time on stream (TOS), the cumulative toluene productivity was, compared to the Re-free Pt/Al_2O_3 system, by 42% and 27% higher for the Re-containing catalysts. Moreover, the Re/Pt = 0.5 catalyst showed an enhanced stability over 20 h TOS, which becomes evident when comparing the achieved conversion levels at 280 °C at different stages of the temperature program. TGA analysis (see SI Fig. A5) revealed a reduction in coke formation from (5.6 ± 0.2) wt% mass loss for the Pt catalysts to (4.9 ± 0.5) wt% and (5.2 ± 0.2) wt% for the systems with Re/Pt = 0.5 and 1.0. This equals to a reduction of 14 and 8%, respectively, and suggests the self-reactivation mechanism proposed by Sachtler.[29] According to this mechanism, Re enhances the ability of reorganising the coke structure on Pt particles, preventing permanent deactivation of active sites. Our results indicate that Re addition increases the selectivity of Pt-based SDP catalysts and reduces coking during MCH dehydrogenation, which is fully aligned with findings from the literature for impregnated systems.[14,30]

Additionally, the kinetics of MCH dehydrogenation were evaluated for the three catalysts. The average hydrogen productivity was calculated for temperatures of 240, 260, 280 (final) and 300 °C and the resulting Arrhenius plot is shown in SI Fig. A6. Notably, Pt–Re catalysts demonstrated lower temperature sensitivity compared to monometallic Pt. From the Arrhenius plots, the effective activation energy was calculated for all systems. For the catalyst with Re/Pt = 0.5, $E_{A,eff}$ was reduced by 19% (59 kJ mol^{-1}) and for Re/Pt = 1.0 by 14% (62 kJ mol^{-1}) in comparison to monometallic Pt (72 kJ mol^{-1}). This supports the assumption of an ensemble effect in Pt–Re systems as reported in the literature, where Re addition divides Pt into smaller ensembles, promoting a single-site mechanism and facilitating the release of H_2.[30]

Table 1 Composition of Pt–Re/Al_2O_3 catalysts prepared *via* the solvent deficient precipitation (SDP) method, as confirmed by ICP-OES analysis, which were tested in the dehydrogenation of methylcyclohexane (MCH)

Pt_{target}/wt%	$Pt_{measured}$/wt%	Re_{target}/wt%	$Re_{measured}$/wt%	Measured Re/Pt molar ratio
0.30	0.29	0	0	0
0.30	0.29	0.15	0.14	0.5
0.30	0.29	0.30	0.27	1.0

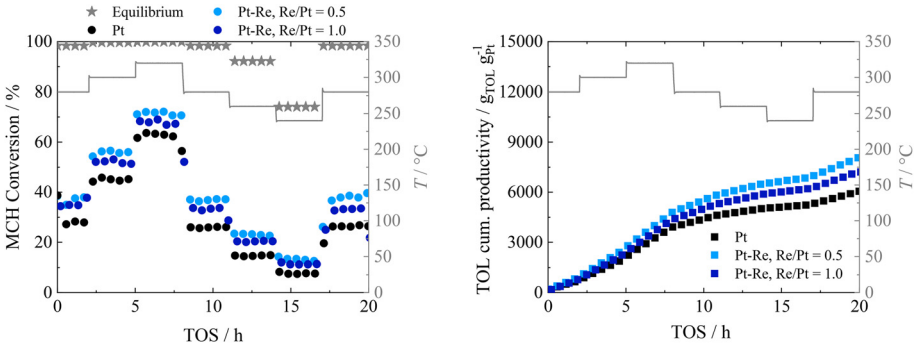

Fig. 9 Methylcyclohexane (MCH) conversion (left) and cumulative productivity from toluene (right) from different Pt–Re/Al_2O_3 catalysts (Re/Pt molar ratios of 0, 0.5 and 1.0) during the dehydrogenation of MCH in the gas phase. Experimental conditions: 1.0 g catalyst, 57 mL min^{-1} He and 0.05 g min^{-1} MCH, WHSV 8.31 L_{gas} h^{-1} g_{cat}^{-1}, 240–320 °C, 1 atm, *ca.* 20 h. Theoretical equilibrium data from Aspen Plus simulation is shown in the left graph.

Table 2 Composition of Pt–Re/Al_2O_3 catalysts prepared *via* the solvent deficient precipitation (SDP) method, as confirmed by ICP-OES analysis, which were tested in the dehydrogenation of perhydro benzyltoluene (H12-BT)

Pt_{target}/wt%	$Pt_{measured}$/wt%	Re_{target}/wt%	$Re_{measured}$/wt%	Measured Re/Pt molar ratio
0.3	0.28	0	0	0
0.3	0.32	0.05	0.03	0.09
0.3	0.30	0.10	0.08	0.28
0.3	0.31	0.15	0.14	0.48
0.3	0.32	0.30	0.27	0.88
0.3	0.29	0.50	0.44	1.60
0.3	0.29	1.00	0.87	3.19

Dehydrogenation in the liquid phase with Pt–Re catalysts

A series of Pt–Re/Al_2O_3 catalysts with Re/Pt molar ratios ranging from 0 to 3.19 was synthesised and tested in the liquid phase dehydrogenation of H12-BT. The Pt and Re contents were determined by ICP-OES and are presented in Table 2. The measured values closely matched the target compositions, with only minor deviations. All subsequent analyses are based on these measured values.

As presented in Fig. 10, the dehydrogenation activity is enhanced for Re containing catalysts with low loadings over the whole course of the reaction. Catalysts with Re/Pt molar ratios exceeding 0.88 demonstrated high initial dehydrogenation rates, which was less evident at higher DoDhs. The analysis of MF formation revealed that these systems led to higher by-product formation. For instance, the catalyst with Re/Pt = 1.60 achieved the highest maximal productivity of 2.9 g_{H_2} g_{Pt}^{-1} min^{-1}, which is 2.3 times higher than the catalyst without Re, but also exhibited significant MF formation (0.15 *vs.* 0.08 mol% at DoDh 27%), likely contributing to the rapid productivity loss observed over time.

To provide a broader overview over the tested range of Re loadings, the average hydrogen productivity was calculated for each catalyst within a DoDh range of 2–25% (see Fig. 11). An optimal Re/Pt molar ratio of 0.5 was identified, yielding an average productivity of 0.85 g_{H_2} g_{Pt}^{-1} min^{-1}. This ratio aligns with the results reported by Strauch *et al.*[15] for the Re/Pt catalysts prepared according to the WI method under similar reaction conditions. Considering that the maximal productivity is reached within the first 5 min of dehydrogenation, this maximum value increased with the Re addition to the catalyst from 0.9 (Re/Pt = 0) to 2.0 g_{H_2} g_{Pt}^{-1} min^{-1} (Re/Pt = 0.5) for our SDP systems. For WI systems, this value increased from 2.0 (Re/Pt = 0) to 4.1 g_{H_2} g_{Pt}^{-1} min^{-1} (Re/Pt = 0.5). For the same Re/Pt molar ratio of 0.5, this represents a 2.3-fold and a 2.1-fold increase for SDP systems and WI systems, respectively. Despite WI systems achieving higher maximal DoDhs and productivity values, the same correlation regarding Re addition to Pt/Al_2O_3 catalysts was observed in SDP systems hinting at a similar activation mechanism. The difference in the absolute productivity values might stem from the small pore size of the SDP catalysts in comparison to the WI counterparts leading to diffusional limitations.[31] A detailed comparison of the corresponding dehydrogenation data between SDP and WI systems can be found in the SI (Fig. A7).

A detailed analysis of the product composition for Pt and Pt–Re systems, shown in SI Fig. A7, revealed that Re containing catalysts with higher Re loadings lead to reduced H6-BT levels. This suggests that Re addition favours the complete dehydrogenation of H12-BT to H0-BT by accelerating the conversion of particularly H6-BT, consistent with findings by Strauch *et al.*[15] with WI Pt–Re catalysts. They attributed these changes in the individual reaction steps to an optimised dispersion of Pt and electronic modification in Pt–Re catalysts. Moreover, an increased formation of MF was

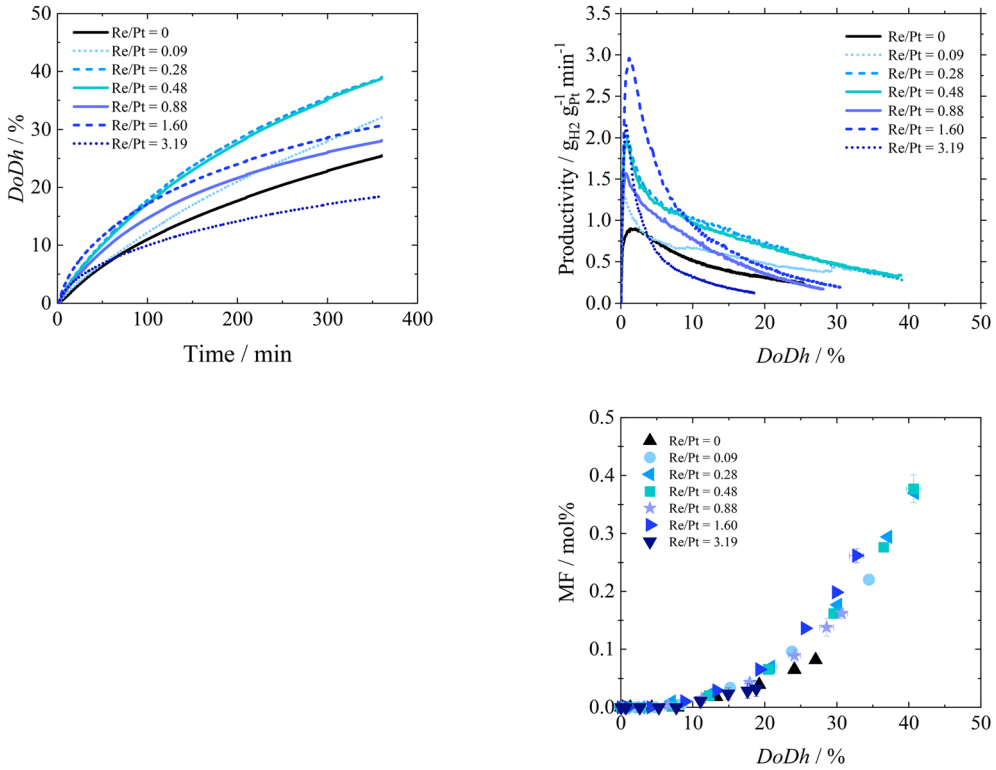

Fig. 10 Degree of dehydrogenation, H_2 productivity and methylfluorene (MF) formation during semi-batch dehydrogenation of perhydro benzyltoluene (H12-BT) with solvent deficient precipitation (SDP) Pt–Re/Al_2O_3 catalysts with different Re/Pt molar ratios. Experimental conditions: T = 250 °C, p = 1 bara, n_{LOHC} = 0.1 mol, w_{Pt} = 0.3 wt%, n_{Pt}/n_{LOHC} = 0.0001, t_R = 360 min, $\dot{V}_{Ar}$ = 300 mL_N min^{-1}. DoDh and productivity data was obtained from TCD measurements, whereas product composition data were determined *via* the GC method. Average values and standard deviation are shown.

observed, which suggests strong binding of the dehydrogenated reaction product H0-BT to the active sites and further dehydrogenation.[15] MF is a consecutive reaction product formed by a deep dehydrogenation step.[32] This can also be seen for the Re containing catalysts in this study and can explain the loss in productivity at higher DoDhs.

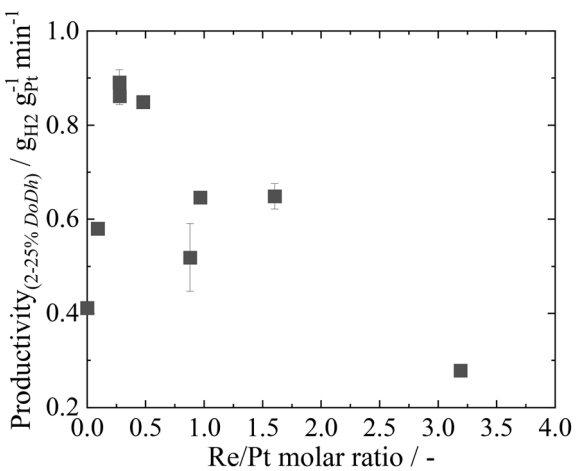

Fig. 11 Average H_2 productivity (calculated from the productivity between a dehydrogenation degree of 2–25%) of different Pt–Re/Al_2O_3 catalysts (Re/Pt = 0–1.60) during dehydrogenation of perhydro benzyltoluene (H12-BT). For Pt–Re catalysts with Re/Pt = 3.19, the average productivity was calculated only up to a DoDh of 18% as no higher levels were reached. Experimental conditions: T = 250 °C, p = 1 bara, n_{LOHC} = 0.1 mol, w_{Pt} = 0.3 wt%, n_{Pt}/n_{LOHC} = 0.0001, t_R = 360 min, $\dot{V}_{Ar}$ = 300 mL_N min^{-1}. Productivity data was obtained from TCD measurements. Average values and standard deviation are shown.

To further investigate the adsorption of aromatic species in Pt–Re systems, the dehydrogenation of a mixture containing 90% H12-BT and 10% H0-BT was conducted with Pt and Re/Pt = 0.5. The results, summarised in Fig. 12, show that when the initial mixture contains H0-BT, the activity of both catalysts is significantly decreased due to the stronger adsorption of H0-BT in comparison to H12-BT[33] and thereby induced blockage of active sites. The average productivity of Pt/Al_2O_3 is reduced from 0.4 to 0.2 g_{H_2} g_{Pt}^{-1} min^{-1}; the catalyst with Re/Pt = 0.5 displays a reduction from 0.9 to 0.3 g_{H_2} g_{Pt}^{-1} min^{-1}. This indicates a strong deactivation effect of H0-BT on the Pt–Re system. Again, for the Re containing catalyst a lower H6-BT fraction can be found at the same DoDh. More interestingly, for the monometallic Pt catalyst the H0-BT fraction remains almost constant over the DoDh range considered, whereas Pt–Re shows a steady increase of H0-BT levels. This supports the finding that the addition of Re to Pt accelerates the dehydrogenation of H6-BT to H0-BT, while H6-BT builds up from the dehydrogenation of H12-BT when using the monometallic catalyst. In addition, an enhanced MF formation can be observed with the Re/Pt = 0.5 catalyst right from the start of the experiment. This points towards

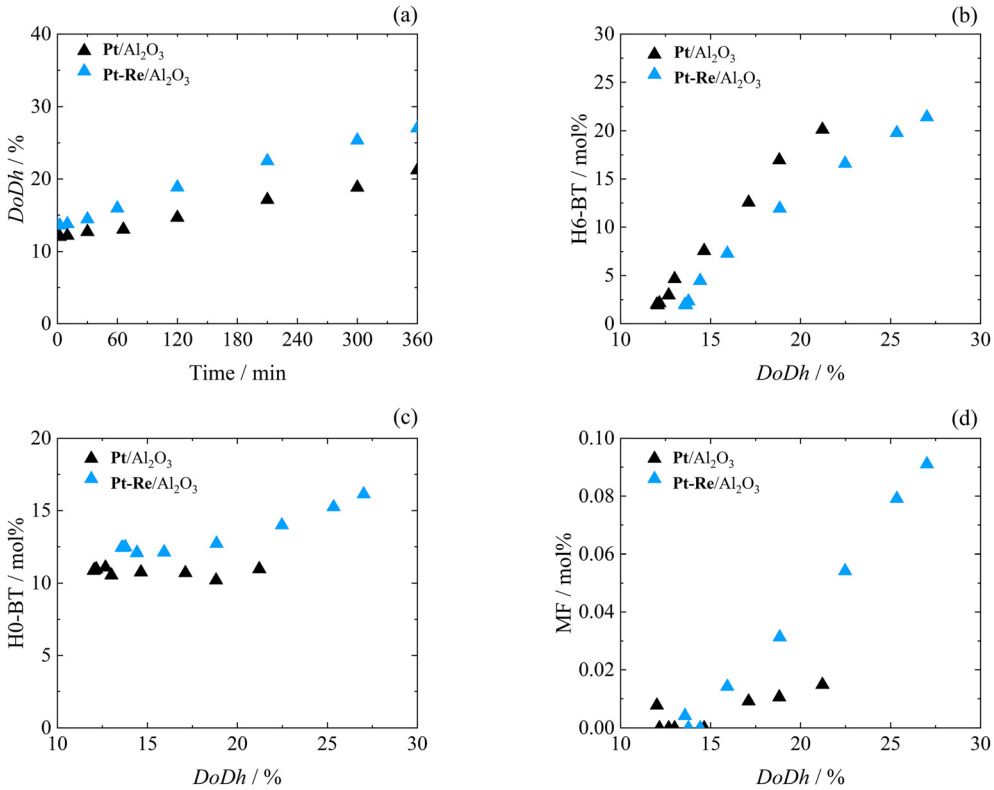

Fig. 12 Degree of dehydrogenation over time (a) and H6-BT (b), H0-BT (c) and methylfluorene (MF) (d) formation as a function of DoDh during the semi-batch dehydrogenation of perhydro benzyltoluene (H12-BT) using Pt/Al_2O_3 and $Pt–Re/Al_2O_3$ (Re/Pt = 0.5) catalysts synthesised *via* the solvent deficient precipitation (SDP) method. Experimental conditions: T = 250 °C, p = 1 bara, n_{LOHC} = 0.1 mol, w_{Pt} = 0.3 wt%, n_{Pt}/n_{LOHC} = 0.0001, t = 360 min, $\dot{V}_{Ar}$ = 300 mL min^{-1}. DoDh and product composition were determined *via* GC analysis.

a further reaction of H0-BT through deep dehydrogenation on the Pt–Re system as discussed before. Overall, the experiments with added H0-BT support the observations made previously in a fully conclusive manner.

The kinetics of H12-BT dehydrogenation for the SDP systems were evaluated for Pt and Pt–Re (molar ratio of 0.5) catalysts at temperatures of 230, 240 and 250 °C. The dehydrogenation data, shown in SI Fig. A9, revealed that the reaction rate of Pt/Al_2O_3 exhibited greater sensitivity to temperature changes compared to $Pt–Re/Al_2O_3$ due to the excellent low-temperature activity of Re-promoted catalysts.[15] The average productivity within 2–25% DoDh was calculated for each temperature and the corresponding Arrhenius plot, shown in SI Fig. A10, enabled the determination of the effective activation energy ($E_{A,eff}$), as presented in SI Table A1. The mean $E_{A,eff}$ for the Pt–Re system (113.0 ± 11.5 kJ mol^{-1}) was found 11% lower than for Pt (126.6 ± 13.7 kJ mol^{-1}). Comparatively, for WI catalysts, the addition of Re resulted in a reduction of 6% (−182.2 kJ mol^{-1} for Pt/Al_2O_3 and −170.5 kJ mol^{-1} for $Pt–Re/Al_2O_3$ with Re/Pt = 0.5),[34] which also reveals a lower effective activation energy in SDP systems in general. This observation suggests that the dehydrogenation with SDP catalysts occurs in the transport-limited regime due to the small pore size of the alumina support in the present study (6 nm).[35] Nevertheless, the general trend regarding reaction kinetics for the addition of Re to Pt/Al_2O_3 catalysts is consistent for WI and SDP catalysts.

Qualitative assessment of mobility of Pt and Re during calcination

To assess possible inhomogeneities during up-scaling and to better understand the Pt–Re and Re–Al interactions during SDP synthesis, the mobility of Pt and Re species was evaluated during calcination. Two experimental approaches were employed following the grinding phase of the synthesis. In the first, the wet solid was shaped into a spherical body and directly calcined. In the second, the solid was dried overnight before being crushed, spread into a crucible and calcined. The results, presented in Table 3, indicate that Pt and Re species are mobile during calcination, as evidenced by variations in their concentrations between the outer shell and inner region of the calcined sphere. However, the molar ratio of Re/Pt remained constant across both approaches and between the outer and inner regions of the spherical catalyst.

Synthesis scale up

To scale up the synthesis, a glass flask and a precision agitator powered by an electrical motor (core-drawn precision glassware, KPG mixer) were used instead of a mortar and pestle. Details on the scale up process can be found in the SI.

Table 3 Images of the resulting materials after the calcination experiment to test Re mobility and corresponding composition as confirmed by ICP-OES analysis

	Sphere	Spread
Before calcination	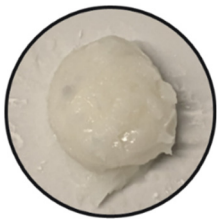	
After calcination	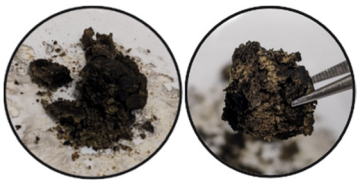	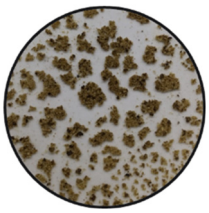
	Outside = 2.88 wt% Pt, 0.91 wt% Re Inside = 1.96 wt% Pt, 0.64 wt% Re	2.70 wt% Pt, 0.91 wt% Re
Molar ratio Re/Pt	Outside = 0.3 Inside = 0.3	0.3

To assess its effectiveness, 3 g of Pt/Al_2O_3 catalyst were synthesised using the KPG setup. The yield was 97% and similar synthesis stages were observed like for the small-scale method with mortar and pestle, including liquefaction, bubbling and precipitation of a wet solid.

The synthesis was scaled up to prepare 40 g of Pt/Al_2O_3 and 30 g $Pt–Re/Al_2O_3$ catalysts. A freeze-drying step was included to remove excess moisture and prevent the extensive displacement of decomposition gases and inhomogeneous drying during calcination (see Table A2) due to the large material volume, which could lead to inhomogeneous products. Neither the longer reaction time of scaled batch sizes nor the freeze-drying step affected the achieved specific surface area and pore size distribution remarkably. The exact compositions of the obtained materials are shown in Table 4.

The catalysts were tested in the dehydrogenation of H12-BT and the results are summarised in Fig. 13. The Pt/Al_2O_3 system achieved an average H_2 productivity of 0.51 g_{H_2} g_{Pt} min^{-1} within the DoDh range of 2–25%, while the Pt–Re system reached 0.97 g_{H_2} g_{Pt} min^{-1}, nearly doubling the productivity with the presence of Re at a Re/Pt molar ratio of 0.43. A comparison with the Pt/Al_2O_3 and $Pt–Re/Al_2O_3$ catalysts from the small-scale synthesis *via* manual grinding is also shown indicating only minimal performance deviations and therefore successful up-scaling. The small deviations most probably stem from the slightly different Pt-loadings and Pt/Re molar ratios between the catalysts synthesized *via* mortar & pestle and KPG mixing.

4. Summary and outlook

This study demonstrates the feasibility of producing $Pt–Re/Al_2O_3$ catalysts *via* the SDP method that show attractive performance in the dehydrogenation of the LOHC compounds methylcyclohexane and perhydro benzyltoluene. Thereby, similar effects as for wet impregnated Pt–Re catalysts could be observed, which highlights the transferability of results between the two different synthesis approaches. Analytical characterization reveals similar textural properties than for pure SDP Al_2O_3 materials with specific surface areas of approx. 300 m^2 g^{-1} and pore sizes in the range of 5 nm. Moreover, small metallic nanoparticles (in the range of 1.8 nm for pure Pt and 1.4 nm for Pt–Re) and indication for Pt–Re interactions influencing catalytic behavior were found.

In the continuous gas-phase dehydrogenation of MCH, the presence of Re enhances activity and selectivity, reduces coking, and promotes catalyst stability. After 20 hours of time on stream, the cumulative toluene productivity was higher by 42% for a catalyst with Re/Pt = 0.5 in comparison to monometallic Pt/Al_2O_3, whereas coke formation was reduced

Table 4 Composition of Pt/Al_2O_3 and $Pt–Re/Al_2O_3$ catalysts prepared *via* the solvent deficient precipitation (SDP) method with a core drawn precision glassware (KPG) mixer (scaled up syntheses), as confirmed by ICP-OES analysis

System	Pt/wt%	Re/wt%	Re/Pt molar ratio	Amount synthesised
Pt	0.24	0	—	40 g (increase by factor 13)
Pt–Re	0.30	0.13	0.43	30 g (increase by factor 10)

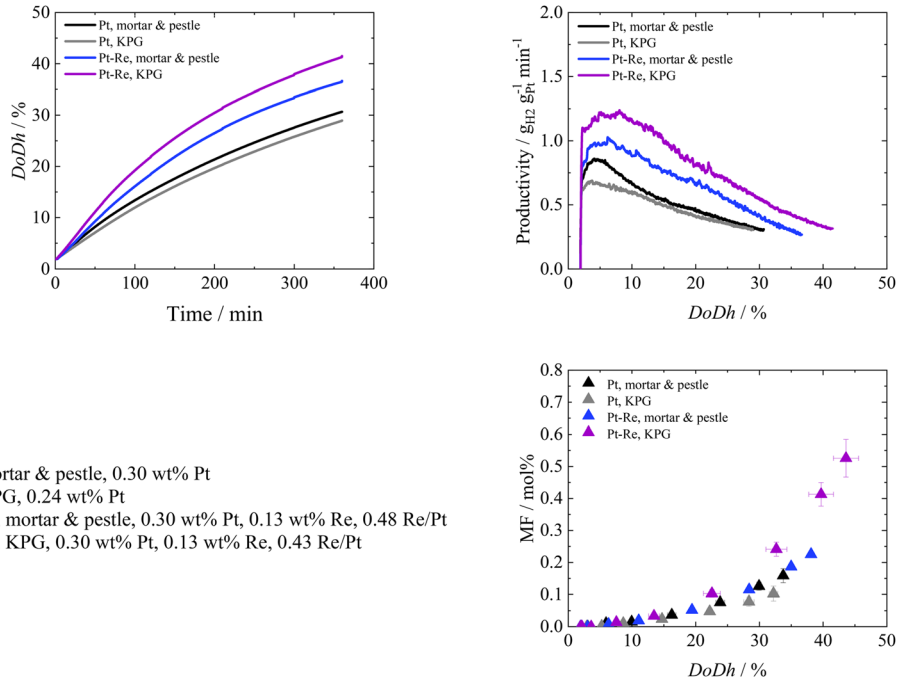

Fig. 13 Degree of dehydrogenation, H_2 productivity and methylfluorene (MF) formation during dehydrogenation of perhydro benzyltoluene (H12-BT) with solvent deficient precipitation (SDP) Pt/Al_2O_3 and $Pt–Re/Al_2O_3$ catalysts synthesised either with a mortar & pestle or with a core drawn precision glassware (KPG) mixer. Experimental conditions: T = 250 °C, p = 1 bara, n_{LOHC} = 0.1 mol, w_{Pt} = 0.3 wt%, n_{Pt}/n_{LOHC} = 0.0001, t_R = 360 min, $\dot{V}_{Ar}$ = 300 mL min^{-1}. DoDh and productivity data was obtained from TCD measurements, whereas product composition data was determined *via* GC method.

by 14%. Kinetic analyses reveal that Re lowers the effective activation energy of the reaction.

In the dehydrogenation of H12-BT, Re addition increased catalyst activity across most tested Re/Pt molar ratios loadings, with Re/Pt = 0.5 yielding the highest average hydrogen productivity (2–25% DoDh) of 0.85 g_{H_2} g_{Pt}^{-1} min^{-1}. This trend aligns with previous findings for WI catalysts. Catalysts containing Re demonstrated higher initial dehydrogenation rates and maintained better performance over the course of the semi-batch reactions compared to Re-free Pt catalysts. However, higher Re loadings (Re/Pt $>$ 0.8) led to rapid productivity decline, likely due to increased formation of by-products, such as MF. The formation of MF and the accumulation of H0-BT suggest that Re facilitates the complete dehydrogenation pathway but also accelerates deep dehydrogenation to MF isomers that causes catalyst deactivation. Experiments with initial H0-BT in the feedstock confirmed that H0-BT inhibits catalyst activity due to its strong adsorption, especially on Re-promoted catalysts. Kinetic studies showed that Re reduces the effective activation energy with SDP catalysts showing diffusional limitations because of their small pore sizes.

Successful upscaling of the SDP synthesis to 10-fold batch size was demonstrated without the need for water, binders, or additives. The scale-up produced catalysts with performances comparable to small-scale samples, confirming the robustness and reproducibility of the synthesis approach. Overall, the results highlight the potential of the SDP method for high-throughput and large-scale experiments, effectively producing suitable bimetallic catalysts and mimicking trends also observed in WI catalysts. SDP proves to be a simple, cost-effective, and scalable 'one-pot' method for preparing both monometallic and bimetallic Pt-based catalysts by co-adding support and active phase precursors.

Conflicts of interest

Peter Wasserscheid is founder and minority shareholder of the company Hydrogenious LOHC technologies (https://www.hydrogenious.net) that offers commercially hydrogen storage systems based on the LOHC technology. There is no conflict of interest to declare about the specific scientific results reported in this paper.

Data availability

Data for this article are available at Zenodo under https://doi.org/10.5281/zenodo.18078485.

Supplementary information (SI) is available. See DOI: https://doi.org/10.1039/d5cy01600b.

Acknowledgements

This work was funded by the Bavarian Ministry of Economic Affairs, Regional Development and Energy through the project "Erforschung und Entwicklung eines emissionsfreien und stark emissionsreduzierten Antriebssystems am Beispiel des

Schienenverkehrs". The authors would like to thank Dr. Andreas Hutzler, Dr. Birk Fritsch and M.Sc. Andreas Körner for obtaining the TEM images of the synthesized catalysts, Dr. Katharina Volz and Dr. Luca Lucarelli from Micromeritics for conducting the CO-pulse chemisorption analysis, M.Sc. Timo Schärfe for developing the Python method to analyse the GC results for H12-BT dehydrogenation, M.Sc. Oshin Sebastian for pre-calibrating the GC used during the off-gas analysis of the MCH dehydrogenation.

References

1 P. Preuster, C. Papp and P. Wasserscheid, *Acc. Chem. Res.*, 2017, **50**, 74.
2 M. M. Distel, J. M. Margutti, J. Obermeier, A. Nuß, I. Baumeister, M. Hritsyshyna, A. Weiß and M. Neubert, *Energy Technol.*, 2025, **13**, 2301042.
3 T. Rüde, A. Bösmann, P. Preuster, P. Wasserscheid, W. Arlt and K. Müller, *Energy Technol.*, 2018, **6**, 529.
4 D. Teichmann, K. Stark, K. Müller, G. Zöttl, P. Wasserscheid and W. Arlt, *Energy Environ. Sci.*, 2012, **5**, 9044.
5 F. Auer, D. Blaumeiser, T. Bauer, A. Bösmann, N. Szesni, J. Libuda and P. Wasserscheid, *Catal. Sci. Technol.*, 2019, **9**, 3537.
6 P. Perreault, L. van Hoecke, H. Pourfallah, N. B. Kummamuru, C.-R. Boruntea and P. Preuster, *Curr. Opin. Green Sustainable Chem.*, 2023, **41**, 100836.
7 M. G. Rasul, M. Hazrat, M. A. Sattar, M. I. Jahirul and M. J. Shearer, *Energy Convers. Manage.*, 2022, **272**, 116326.
8 Q. N. Dao, E. On, S. Ramadhani, K. Lee, H. Sohn, S. H. Choi, S. Y. Lee, H. Jeong and Y. Kim, *Int. J. Hydrogen Energy*, 2024, **56**, 1284.
9 J. Oh, Y. Jo, T. W. Kim, H. B. Bathula, S. Yang, J. H. Baik and Y.-W. Suh, *Appl. Catal., B*, 2022, **305**, 121061.
10 J. Barbier, *Appl. Catal.*, 1986, **23**, 225.
11 D. Y. Murzin, *Engineering Catalysis*, de Gruyter, Berlin, Boston, 2013.
12 P. Biloen, J. N. Helle, H. Verbeek, F. M. Dautzenberg and W. Sachtler, *J. Catal.*, 1980, **63**, 112.
13 K. Jothimurugesan, S. Bhatia and R. D. Srivastava, *Ind. Eng. Chem. Fundam.*, 1985, **24**, 433.
14 M. S. Akram, R. Aslam, F. S. Alhumaidan and M. R. Usman, *Int. J. Chem. Kinet.*, 2020, **52**, 415.
15 D. Strauch, P. Weiner, B. B. Sarma, A. Körner, E. Herzinger, P. Wolf, A. Zimina, A. Hutzler, D. E. Doronkin, J.-D. Grunwaldt, P. Wasserscheid and M. Wolf, *Catal. Sci. Technol.*, 2024, **14**, 1775.
16 B. F. Woodfield, S. Liu, J. Boerio-Goates and Q. Liu, *WO Pat.*, WO/2007/098111, 2007.
17 S. J. Smith, B. Huang, S. Liu, Q. Liu, R. E. Olsen, J. Boerio-Goates and B. F. Woodfield, *Nanoscale*, 2015, **7**, 144.
18 B. L. Cushing, V. L. Kolesnichenko and C. J. O'Connor, *Chem. Rev.*, 2004, **104**, 3893.
19 J. Oh, H. B. Bathula, J. H. Park and Y.-W. Suh, *Commun. Chem.*, 2019, **2**, 1.
20 Y. Jo, T. Wan Kim, J. Oh, D. Kim and Y.-W. Suh, *J. Catal.*, 2022, **413**, 127.
21 Y. Jo, D. Kim, T. W. Kim, D. Yoon and Y.-W. Suh, *Appl. Catal., B*, 2023, **334**, 122848.
22 J. Schindelin, I. Arganda-Carreras, E. Frise, V. Kaynig, M. Longair, T. Pietzsch, S. Preibisch, C. Rueden, S. Saalfeld and B. Schmid, *et al.*, *Nat. Methods*, 2012, **9**, 676.
23 M. Alderliesten, *Part. Part. Syst. Charact.*, 1991, **8**, 237.
24 O. Sebastian, S. Nair, N. Taccardi, M. Wolf, A. Søgaard, M. Haumann and P. Wasserscheid, *ChemCatChem*, 2020, **12**, 4533.
25 Aspen Technology Inc., *Aspen Plus*, aspenONE Engineering, 2020.
26 C. L. Pieck, C. R. Vera, J. M. Parera, G. N. Giménez, L. R. Serra, L. S. Carvalho and M. C. Rangel, *Catal. Today*, 2005, **107–108**, 637.
27 K. G. Azzam, I. V. Babich, K. Seshan, B. L. Mojet and L. Lefferts, *ChemCatChem*, 2013, **5**, 557.
28 C. G. Michel, W. E. Bambrick, R. H. Ebel, G. Larsen and G. L. Haller, *J. Catal.*, 1995, **154**, 222.
29 W. M. H. Sachtler, *J. Mol. Catal.*, 1984, 1.
30 P. A. Van Trimpont, G. B. Marin and G. F. Froment, *Ind. Eng. Chem. Fundam.*, 1986, **25**, 544.
31 F. Auer, T. Solymosi, C. Erhardt, C. C. Collados, M. Thommes and P. Wasserscheid, *Int. J. Hydrogen Energy*, 2025, **100**, 1282.
32 T. Rüde, S. Dürr, P. Preuster, M. Wolf and P. Wasserscheid, *Sustainable Energy Fuels*, 2022, **6**, 1541.
33 M. Geißelbrecht, S. Mrusek, K. Müller, P. Preuster, A. Bösmann and P. Wasserscheid, *Energy Environ. Sci.*, 2020, **13**, 3119.
34 D. Strauch, *PhD thesis*, Friedrich-Alexander-Universität Erlangen-Nürnberg, 2023.
35 A. Jess and P. Wasserscheid, *Chemical Technology: An Integral Textbook, Zweite, erweiterte Auflage*, Wiley-VCH, Weinheim, Germany, 2013.